Intersite comparison of interannual nearshore bar behavior

B. G. Ruessink,[1] K. M. Wijnberg,[2] R. A. Holman,[3] Y. Kuriyama,[4] and I. M. J. van Enckevort[1]

[1] Long-term (>years) bathymetric data sets collected in six multiple near-shore sandbar systems were analyzed with complex empirical orthogonal function analysis to quantify intersite differences and similarities in cyclic offshore progressive bar behavior. The observations came from a 37-year annually sampled data set of four regions along the Dutch coast (spanning 70 km of coastline), an 18-year fortnightly to monthly sampled data set at Duck, North Carolina (alongshore extent ∼1 km), and a 7-year daily sampled data set of a single cross-shore profile at the Hasaki coast of Japan. The first complex mode, typically representing 50–70% of the total depth variance, described the long-term offshore progressive behavior and allowed for an objective separation of the barred part of the profile from the shoreward- and seaward-located nonbarred parts by considering a threshold bar amplitude below which the spatial results from the first mode were not considered reliable. The sandbars at the six examined sites share common lengths and nondimensional amplitude characteristics, which can be described by a negatively skewed Gaussian function. The absolute amplitude dimensions and the cycle return intervals differ, however, considerably between the sites. The key geometric parameters that steer this intersite variation are the time-averaged mean depths at the shoreward and seaward side of the bar zone ($\overline{d}_{\text{shore}}$ and $\overline{d}_{\text{sea}}$, respectively) as well as their difference $\overline{d}_{\text{bz}}$. The degree to which intersite differences in $\overline{d}_{\text{shore}}$, $\overline{d}_{\text{sea}}$, and $\overline{d}_{\text{bz}}$ are related linearly to intersite differences in bulk statistics of external forcings (wave, tide, sediment, and bed profile characteristics) is inconclusive.   INDEX TERMS: 3020 Marine Geology and Geophysics: Littoral processes; 3099 Marine Geology and Geophysics: General or miscellaneous; 4546 Oceanography: Physical: Nearshore processes; KEYWORDS: sandbars, nearshore morphology, bathymetry, eigenfunction analysis

1. Introduction

[2] Alongshore bars are submarine ridges of sand, typically located in water depths of less than 10 m and oriented approximately parallel to the shoreline. They have a multi-annual lifetime and occur singularly or in multiples of up to 4 or 5 bars, extending for up to several tens of kilometers along the shore. They have been observed fringing coasts along large lakes [e.g., *Evans*, 1940; *Saylor and Hands*, 1970], semienclosed seas [e.g., *Greenwood and Davidson-Arnott*, 1975; *Ruessink and Kroon*, 1994; *Wijnberg and Terwindt*, 1995], and open oceans [e.g., *Lippmann et al.*, 1993; *Shand and Bailey*, 1999; *Kuriyama and Lee*, 2001]. The natural variability in the cross-shore and alongshore appearance of bars, and changes therein, is stunning [e.g., *Zenkovich*, 1967], and includes variability in spatial (in the cross-shore) characteristics, such as bar amplitude and bar length, and long-term (>years) temporal characteristics. While considerable work has been done in quantifying these characteristics at individual sites [e.g., *Greenwood and Davidson-Arnott*, 1975; *Larson and Kraus*, 1994; *Ruessink and Kroon*, 1994; *Pruszak et al.*, 1997; *Plant et al.*, 1999], studies comparing the sites are limited and are hampered by the multiplicity of applied analysis techniques. As a result, factors controlling the intersite variability in spatial and temporal sandbar behavior are not well understood.

[3] The description of spatial characteristics of barred cross-shore profiles has often been organized as a description of geometric parameters, like bar amplitude, bar length, bar volume, bar zone width, or water depth above the crest. These parameters have either been computed directly from bathymetric surveys [e.g., *Keulegan*, 1948; *Shepard*, 1950; *Saylor and Hands*, 1970; *Ruessink and Kroon*, 1994; *Plant et al.*, 1999] or from functions fitted to the data [*Pruszak and Różyński*, 1998; *Plant et al.*, 2001]. There is consider-

[1]Institute for Marine and Atmospheric Research, Department of Physical Geography, Utrecht University, Utrecht, Netherlands.
[2]WL|Delft Hydraulics, Marine and Coastal Management, Delft, Netherlands.
[3]Coastal Imaging Laboratory, College of Oceanic and Atmospheric Sciences, Oregon State University, Corvallis, Oregon, USA.
[4]Littoral Drift Division, Marine Environment and Engineering Department, Port and Airport Research Institute, Yokosuka, Japan.

able debate in the literature about environmental factors controlling intersite differences in geometric parameters. *Zenkovich* [1967, p. 233] noted that "convincing proof has been obtained in the eastern Baltic of the absence of any direct connection between the structure of bars and such important elements as the amount of material in movement and the parameters of storm waves." In contrast, *Larson and Kraus* [1989] linked differences in geometric bar properties in the laboratory to the offshore wave height and period, and to the sediment fall velocity. Also, *Davidson-Arnott* [1988] suggested after a comparative study of bar systems in the lower Great Lakes and the Gulf of St. Lawrence that the depth above the outer bar increases linearly with increasing maximum wave height. Measurements of wave height were, however, unavailable in this study and the maximum wave height was therefore inferred from the longest fetch length within 45° from shore normal. Interestingly, there also appears to be some similarity in geometric parameters between the sites. For instance, the ratio of the water depth in the trough to the depth above the next seaward-located bar crest has often been reported to attain an approximately constant value of 1.7 [*Keulegan*, 1948; *Shepard*, 1950; *Saylor and Hands*, 1970; *Greenwood and Davidson-Arnott*, 1975], although a positive dependence of this ratio on the offshore wave steepness has also been found [*King*, 1959; *Larson and Kraus*, 1989]. Additionally, *King and Williams* [1949] noted that the water depth over the bar crest to the height of the bar crest above a smooth barless profile has a ratio of 2 to 1. A similar value can also be deduced from the laboratory bar profiles reported by *Keulegan* [1948] and the field data by *Shepard* [1950] and *Zenkovich* [1967]. Outer bars often disobey these ratios [e.g., *King*, 1959], as they tend to be more subdued than inner bars. Finally, in multiple bar settings, the depth over the bar crest often increases linearly over successive bars, while the spacing between crests increases exponentially in the offshore direction [e.g., *Saylor and Hands*, 1970; *Pruszak et al.*, 1997].

[4] Long-term sandbar behavior often has a cyclic offshore directed character [*Ruessink and Kroon*, 1994; *Wijnberg and Terwindt*, 1995; *Plant et al.*, 1999; *Shand and Bailey*, 1999; *Kuriyama and Lee*, 2001]. A bar cycle comprises bar generation near the shoreline, net offshore migration through the surf zone, and bar decay at the seaward margin of the nearshore. Bar decay is associated with the onset of net offshore migration of the next shoreward-located bar and bar birth near the shoreline. This type of behavior may be alongshore coherent for >10 km [*Wijnberg and Terwindt*, 1995; *Wijnberg*, 1998] and, accordingly, reflects cross-shore oriented bar variability, in other words, does not result from the alongshore propagation of shore oblique bars. Reported cycle return period range from about 1 year at the Pacific Coast of Japan [*Kuriyama and Lee*, 2001] to well over 10 years along the Dutch Coast [*Ruessink and Kroon*, 1994; *Wijnberg and Terwindt*, 1995]. *Shand et al.* [1999] suggested that the duration of net offshore migration (i.e., the time period between the onset of this migration trend and the onset of bar decay) decreases with increasing nearshore slope, decreasing wave height, and a predominant wind direction tending to a maximum of 40 to 45° with the coastline. These duration/process relationships should be interpreted with caution. Not only were the intersite differences in process parameters small compared to the wide

Table 1. Data Set Characteristics

Region	Extent,[a] km	Spacing,[a] m	Time Period	N[b]	x_{end},[c] m	N_w[d]
Zuid-Holland	35	250	1964–2000	37	850	35
Noord-Holland	24	250	1964–2000	37	1100	24
Terschelling	4	200	1965–2000	36	1700	4
Ameland	7	200	1964–2000	37	1400	7
Duck	1.2[e]	45	1981–2000	492	400	1
Hasaki	0	–	1987–1994	2150	400	1

[a]In the alongshore direction.
[b]Number of temporal observations.
[c]Most seaward cross-shore coordinate.
[d]Number of alongshore windows in which data was analyzed; see section 3.
[e]Here 400 m was discarded because of pier effects.

range of duration values, but also the duration and process parameters were not computed in the same consistent manner in *Shand et al.*'s [1999] literature sources.

[5] In this paper we quantify intersite differences and similarities in geometric and long-term temporal bar characteristics from long-term bathymetric data sets available for 6 different sites with known offshore progressive bar behavior. The data (section 2) came from 4 regions along the Dutch coast, Duck on the eastern US seaboard, and the Hasaki Coast of Japan. Complex empirical orthogonal function analysis (section 3) was applied to quantify the cross-shore evolution of bar amplitude and bar length, and the return period of successive bar decay at the outer edge of the nearshore. The present work is unique in the sense that it analyzes a large number of the existing long-term bathymetric data sets of nearshore bars with a single technique, thereby allowing for a proper intersite comparison of geometric and temporal bar characteristics. The results of this comparison can be found in section 4, in which attention is, in particular, focused on the similarity in geometric parameters. Section 5 explores the possible role of wave, tide, sediment, and bed profile characteristics on the observed intersite differences in bar amplitude and return period. Finally, our main conclusions are discussed and summarized in sections 6 and 7, respectively.

2. Field Sites and Data Set Description

[6] Bathymetric data sets analyzed in this paper were collected in four regions along the Dutch coast, near Duck, North Carolina, and on the Hasaki Coast of Japan (Table 1). Each of the sites is characterized by the presence of a sandbar system that behaves in a cyclic, offshore directed manner. Earlier analyses of the data, together with extensive descriptions of the field sites and of the data set characteristics, are given by *Ruessink and Kroon* [1994] and *Wijnberg and Terwindt* [1995] for the Dutch coast, by *Lippmann et al.* [1993] and *Plant et al.* [1999] for Duck, and by *Katoh* [1998] and *Kuriyama* [2000, 2002] for Hasaki.

[7] Data collected at the four Dutch regions (Zuid-Holland, Noord-Holland, Terschelling, and Ameland) form part of the Jarkus data base, which contains annual surveys since 1964 using vertical aerial photogrammetry and echo-sounding. Alongshore spacing between cross-shore depth profiles is 200–250 m (Table 1). Up to 1985, all surveys extended 800 m offshore, and often missed the seaward end

of the bar zone, particularly at Terschelling and Ameland. Since 1985, profiles have been surveyed up to several kilometers off the beach, well seaward of the bar zone. The Zuid-Holland and Noord-Holland region are located on the approximately 120-km long, inlet-free Holland Coast, and are separated by the IJmuiden harbor jetties, which extend about 2.5 km into the sea. Terschelling and Ameland are barrier islands located in the northern part of the Netherlands. Analyzed data is located in front of the central part of the islands, in between the outer deltas associated with the tidal inlet systems that separate the barrier islands.

[8] Data collection at the U.S. Army Corps of Engineers Field Research Facility (FRF) near Duck, located on a barrier island in the Atlantic Ocean, started in 1981 and has continued at approximately fortnightly to monthly intervals. The data, obtained with an amphibious vehicle, spans roughly 1 km alongshore, centered about the FRF pier, and mostly extends sufficiently far offshore to include all depth variability related to the sandbars. Data within 200 m of the pier was excluded from the analyses because of the effect of the pier on the morphology [*Plant et al.*, 1999]. Alongshore spacing between cross-shore depth profiles in the remaining northern and southern part is about 45 m.

[9] The Hasaki data comprises depth profiles of a single cross-shore transect along the Hazaki Oceanographical Research Station, a 427 m long pier facing the Pacific Ocean. The profiles were collected on a daily basis (except for weekends and holidays) between 1987 and 1994 using a 5 kg lead from the pier, and with level and staff shoreward of the pier. On the basis of a limited number of bathymetric surveys in a 600-m alongshore region centered about the HORS pier, *Kuriyama* [2000] showed that the mean profile and the standard deviation of the seabed along HORS were almost identical to that further away from the pier, in other words, that the Hasaki data, despite being measured from a pier, is representative of open beach dynamics. This is in marked contrast with the FRF pier, where scour around pilings has resulted in a pronounced shore perpendicular trough and in a standard deviation about twice as high as further away from the pier. The FRF pier is supported by double pilings, while the HORS pier is supported by single pilings, probably explaining why the Hasaki data does not appear to be much influenced by the presence of the pier. The bar zone ends near the tip of the HORS pier [*Kuriyama*, 2002].

[10] At all sites individual survey points were taken at varying distances from a local baseline. Linear interpolation was therefore employed to yield depth estimates at common cross-shore points. The cross-shore distance between consecutive grid points was set to 5 m. In each cross-shore profile, $x = 0$ was set to the cross-shore location with a height of +1 m above mean sea level; this height approximates the mean high tide level at all sites. The +1 m height can be considered as a process-oriented reference height, separating the subaerial part of the profile from the subaqueous part. The subaqueous part is subject to hydrodynamic processes on a daily timescale, whereas the subaerial part is submerged during storms only. The +1 m contour was preferred over some deeper located datum (e.g., mean sea level or the low-tide level) because its position is less sensitive to large short-term (days-seasons) fluctuations. The concept of a floating datum was previously applied by *Wijnberg and Terwindt* [1995] in a conventional EOF analysis of the Zuid-Holland

and Noord-Holland data. They found that apparent bar movement induced by the floating datum was negligible because generally less than 10% of the variation in bar position was correlated with a change in the +1 m position. The most seaward cross-shore coordinate included in the data set, x_{end}, was based on the standard deviation $\sigma(x)$ of the depth values. In the zone where bars were active σ was typically high, dropping off rapidly to an approximately constant value farther offshore [e.g., *Ruessink and Kroon*, 1994; *Plant et al.*, 1999], related largely to measurement errors. For each region, x_{end} was chosen such (Table 1) that this change to a constant σ was just included in all cross-shore profiles.

3. Methodology

[11] At each alongshore (y) position the time-distance matrix of seabed surface $z_b(t, x)$, where t denotes time, is composed of a mean (in time) profile $\bar{z}_b(x)$ and perturbations $\tilde{z}_b(t, x)$ around $\bar{z}_b(x)$,

$$z_b(t,x) = \bar{z}_b(x) + \tilde{z}_b(t,x). \qquad (1)$$

The perturbation matrix, in turn, consists of cross-shore coherent bar behavior $\tilde{z}_{bar}(t, x)$ and ambient noise $\epsilon(t, x)$,

$$\tilde{z}_b(t,x) = \tilde{z}_{bar}(t,x) + \epsilon(t,x). \qquad (2)$$

The noise term consists of measurement errors as well as depth changes that are not coherent across the profile. The quantification of $\tilde{z}_{bar}(t, x)$ from $z_b(t, x)$ requires the computation of the mean profile and the separation of the coherent bar variability from the noise. This separation is achieved by a complex empirical orthogonal function (CEOF) analysis, decomposing $\tilde{z}_b$ into complex spatial functions and associated complex coefficients. This analysis has the ability to detect propagating wave phenomena and, as all data sets contain offshore propagating bars, is capable of separating the dominant bar behavior from the less dominant noise.

[12] To increase the reliability of the spatial eigenfunctions, we decided not to analyze each cross-shore profile individually, but instead, following *Wijnberg and Terwindt* [1995], to analyze the bathymetric data in windows comprising depth profiles from several alongshore positions (see *North et al.* [1982] and *Horel* [1984] for a discussion on the effect of sample size on the accuracy of eigenfunction results). For the Jarkus data, the window width was set to 1 km. This window was then moved along the coast with a step size of 1 km. The width of the window is assumed to be small enough to still reliably determine large-scale trends (e.g., in mean profile slope) that may affect bar characteristics. The Duck data was treated as a single window, including all cross-shore sections in the region north and south of the FRF pier. Henceforth, all available profiles within a window are denoted as $z_b(t, x)$ and, accordingly, the mean profile refers to a time-averaged and alongshore (within a window)-averaged profile. The Hasaki data can obviously not be analyzed in separate windows, as it comprises a single cross-shore profile. For consistency, we will treat the Hasaki data as a window comprising a single cross section.

[13] Complex EOF is performed on the complex matrix $Z_b(t, x)$, whose real part is the original matrix $\tilde{z}_b(t, x)$ and whose imaginary part is the Hilbert transform of $\tilde{z}_b(t, x)$. The

addition of the Hilbert transform as the imaginary part to $Z_b(t, x)$ allows travelling wave activity in the real field to be detected [*Horel*, 1984]. The same procedure for determining spatial eigenfunctions $E_n(x)$ and temporal coefficients $A_n(t)$ is used as in the more conventional real EOF [e.g., *Von Storch and Zwiers*, 1999], where n is an integer denoting the mode number. Because $\tilde{z}_b(t, x)$ and thus $Z_b(t, x)$ often contained missing observations owing to incomplete surveys, this procedure was accommodated using *Von Storch and Zwiers*'s [1999] approach to handle gappy data. In the present application, the spatial functions carry the units, whereas the coefficients are nondimensional. A rigorous description of CEOF analysis can be found elsewhere [e.g., *Barnett*, 1983; *Horel*, 1984; *Von Storch and Zwiers*, 1999]. Note that the use of windows implies that the CEOF analysis results in one set of spatial eigenfunctions for each window but in temporal coefficients at each alongshore position within a window.

[14] Preliminary analysis of the data [*Kuriyama and Lee*, 2001; *Ruessink et al.*, 2001] has shown that the first complex mode typically accounts for 50–70% of the total variance in $\tilde{z}_b(t, x)$ with percentages increasing to 60–75% in the zone where bars were most active. Because our focus is on properties of coherent bar behavior, $\tilde{z}_{bar}(t, x)$ can be represented adequately in terms of the amplitude and phase of $E_1(x)$ and $A_1(t)$,

$$\tilde{z}_{bar}(t, x) = S(x)R(t)\cos[\theta(x) - \psi(t)], \qquad (3)$$

in which $S(x)$ is the time-invariant spatial envelope of bar amplitude, $R(t)$ represents normalized temporal variations in $S(x)$, and $\theta(x)$ and $\psi(t)$ are the spatial and temporal phase, respectively. $S(x)$ and $R(t)$ are the absolute values of $E_1(x)$ and $A_1(t)$, respectively, and $\theta(x)$ and $\psi(t)$ follow from

$$\theta(x) = \arctan\left[\frac{\Im\{E_1(x)\}}{\Re\{E_1(x)\}}\right] \qquad (4)$$

and

$$\psi(t) = \arctan\left[\frac{\Im\{A_1(t)\}}{\Re\{A_1(t)\}}\right], \qquad (5)$$

where $\Im\{\}$ and $\Re\{\}$ denote the imaginary and real part, respectively. The bar length $L(x)$ is computed as [e.g., *Barnett*, 1983]

$$L(x) = \frac{2\pi}{\nabla\theta(x)} \qquad (6)$$

and the cycle return period T_r equals the ratio of 2π to the slope of the least squares linear fit of ψ versus time.

[15] The interpretation of $S(x)$, $R(t)$, $L(x)$, and T_r is illustrated with the results of the window $y = 41$–42 km in Noord-Holland. Figure 1a shows a space-time map (time stack) of the perturbations at $y = 41.50$ km. Warm colors correspond to perturbations above the window mean and time mean profile (bars), while cold colors corresponds to perturbations below the mean (troughs). Four successive bars can be identified in the 37-year time period, each of which is generated near $x \approx 150$ m, migrates offshore for several years, and finally vanishes near $x \approx 700$ m. The inner bar starts to migrate offshore once the most seaward-

located bar has reached its maximum distance offshore and starts to degenerate (e.g., bars 2 and 3 around 1986). The average bar return period in this example can be estimated at about 15 years. A space-time map of the perturbations reconstructed with the first CEOF, accounting for 57% of the variance, is shown in Figure 1b. The same four bars can be identified, compare Figure 1b with Figure 1a. The amount of explained variance in the bar zone is high, with r^2 (computed with linear regression between measured and reconstructed perturbations) typically larger than 0.6 and maximum r^2 near 0.85 (Figure 2a). Perturbations at $x < \approx 150$ m and $x > \approx 700$ m are poorly resolved by the first CEOF (Figure 1b), with $r^2 < 0.4$ (Figure 2a).

[16] In the example window, S is small at the shoreward and seaward side of the cross-shore profile and large in the middle part ($150 < x < 700$ m), where the bars were active (Figure 2b). Large S are associated with large r^2, compare Figures 2a and 2b. When S and r^2 are small (near the shoreward and seaward end of the cross-shore profile), L estimates (Figure 2d) are rather erratic and do not follow the general increase with distance offshore for $150 < x < 700$ m where S and r^2 are large. To avoid spurious results a threshold $S = 0.3$ m was chosen below which the spatial CEOF results were considered to be unreliable. On the seaward side $S = 0.3$ m is approximately located where σ changes into approximately constant values (section 2) and r^2 drops off rapidly to near-zero values (Figure 2a). The results in the remainder of this paper are not very sensitive to the precise threshold value, since the change from large to low S occurred within rather narrow x ranges (Figure 2b). With the threshold S we have introduced an objective criterion to separate the barred part of the profile from the nonbarred part. We now define a number of simple geometric parameters that are used in section 4 to investigate the similarity in spatial (cross-shore) bar characteristics, viz. the shoreward and seaward limit of the bar zone, x_{shore} and x_{sea}, respectively, the mean depths ($\overline{d} = -\overline{z}_b$) at these locations $\overline{d}_{shore}$ and $\overline{d}_{sea}$, the bar zone width $x_{bz} = x_{sea} - x_{shore}$, the bar zone depth range $\overline{d}_{bz} = \overline{d}_{sea} - \overline{d}_{shore}$, the maximum value of S, S_{max}, and the cross-shore location and mean depth where $S = S_{max}$, x_{max} and $\overline{d}_{max}$, respectively. In the example, $x_{shore} = 130$ m, $x_{sea} = 705$ m, $\overline{d}_{shore} = 1.63$ m, $\overline{d}_{sea} = 6.39$ m, $x_{bz} = 575$ m, $\overline{d}_{bz} = 4.75$ m, $S_{max} = 1.37$ m, $x_{max} = 470$ m, and $\overline{d}_{max} = 4.98$ m.

[17] The temporal results in the example window are plotted in Figure 3. The real and imaginary part of $A_1(t)$ vary repetitive around 0 with a period of ~15 years (Figure 3a), with the imaginary part lagging the real part by several years (about one-quarter wavelength). This pattern reflects the cyclic offshore directed sandbar propagation. The absolute value of A_1, R, shows variability of little interest (Figure 3b) and has a time-averaged value of 1 owing to its normalized nature. The unwrapped temporal phase increases with time (Figure 3c). The slope of the least squares linear fit amounts to 0.45 rad year^{-1} ($r = 0.97$), corresponding to $T_r = 14$ years, close to the 15 years suggested from Figure 1a.

4. Results

[18] In this section we focus on intersite differences and similarities in bar amplitude S, bar length, and cycle
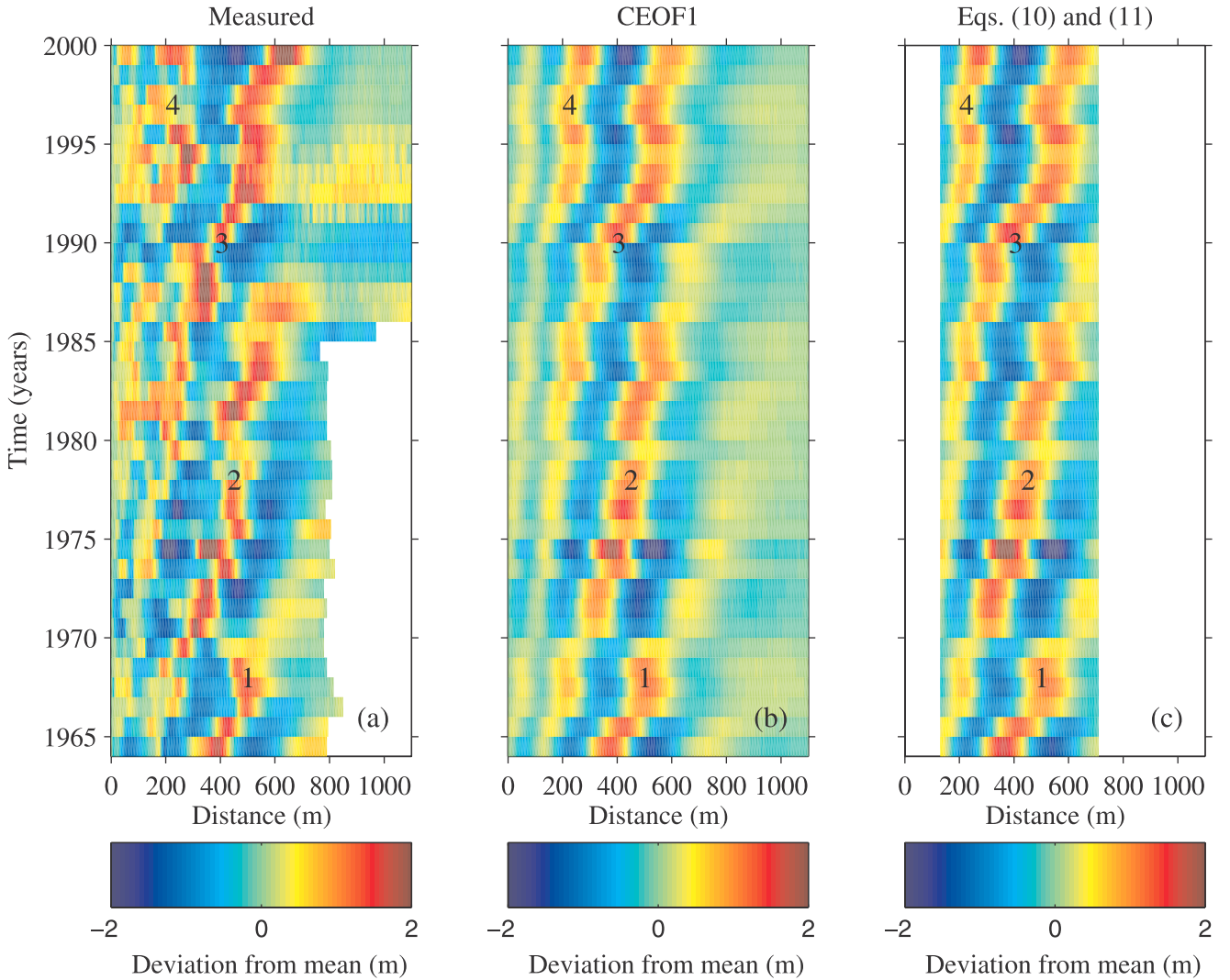
Figure 1. Space-time map of the (a) observed and reconstructed perturbations $\tilde{z}_b(t, x)$ based on (b) CEOF mode 1 and (c) equations (10), (11), and the temporal information of CEOF mode 1 at $y = 41.50$ km in Noord-Holland, Netherlands. Individual sandbars are labeled. Blank regions in Figures 1a and 1c represent missing data and the barless ($S < 0.3$ m) parts of the profile, respectively.

return period. Temporal variations in the bar amplitude are not considered, which implies that bar amplitude is investigated for a typical situation ($R(t) = 1$). Various parameterizations will be developed to highlight the similarity in geometric parameters. These parameterizations are not meant as a replacement for understanding the physics of spatial and temporal sandbar behavior, but instead they capture the essence of our observations both as plausible guidance to further research and as rules of thumb for researchers who wish to represent natural sandbar systems.

4.1. Geometric Characteristics

4.1.1. Bar Amplitude

[19] As can be seen in Figure 4 and Table 2, considerable intersite variability exists for the bar amplitude envelopes S and the related geometric parameters defined in section 3. For instance, at Duck the bar zone extends from $x = 20$ to 270 m in depths of about 1 to 4 m below mean sea level. In contrast, at Terschelling, the bar zone is ≈4 times as wide and extends to about 7-m depth (Table 2). In addition, S_{max} at Terschelling is about twice as large as at Duck. Besides the intersite variability, there also appears to be some small intrasite variability in the Dutch $S(x)$ curves (Figure 4 (left)). However, this variability is less prominent in $S(\overline{d})$ (compare Figure 4 (right) to Figure 4 (left)), implying that S is a function of mean depth rather than of cross-shore distance, and that the noted intrasite variability in $S(x)$ may be related to small slope differences of the window mean cross-shore profile at each site.

[20] The shape of the $S(\overline{d})$ curves is remarkably similar. All curves rise gently from near-zero values up to some maximum and then drop off to near-zero values again. As $\overline{d}_{sea}$ increases (i.e., the bar zone extends into larger depths), S_{max} and $\overline{d}_{max}$ increase as well (Figure 5 and Table 3). To explore the similarity in $S(\overline{d})$ further, site-averaged $S(\overline{d})$ curves were computed for the four Dutch
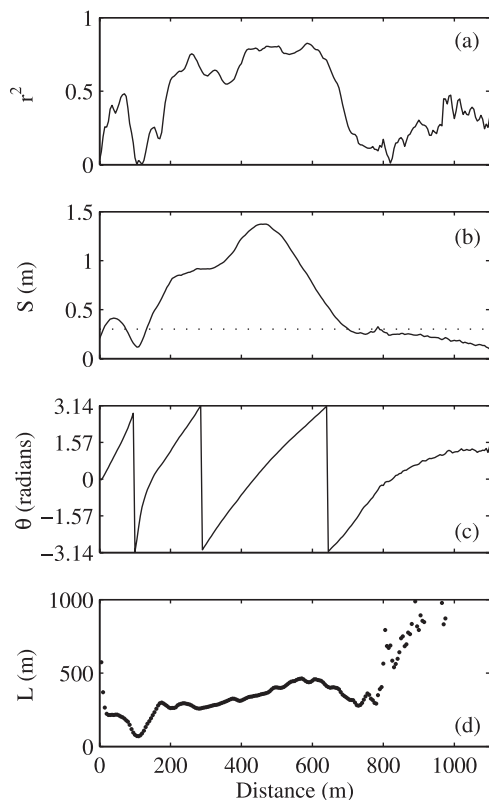
Figure 2. (a) Explained variance r^2, (b) envelope of the bar amplitude S, (c) spatial phase θ, and (d) bar length L versus cross-shore distance x in the example data set ($y = 41 - -42$ km, Noord-Holland). The dotted line in Figure 2b is the threshold $S = 0.3$ m to compute the barred part of the cross-shore profile; see text for further explanation.

sites by binning S corresponding to $\overline{d} \pm 0.05$ m and subsequently normalizing $\overline{d}$ and S for all six sites as

$$d' = \frac{\overline{d} - \overline{d}_{\text{shore}}}{\overline{d}_{\text{sea}} - \overline{d}_{\text{shore}}} \qquad (7)$$

and

$$S' = \frac{S - \delta}{S_{\max} - \delta}, \qquad (8)$$

in which δ is the threshold $S = 0.3$ m. In this way, the bar zone ranges from $d' = 0$ to $d' = 1$, with $S' = 0$ at $d' = 0$, 1 and $S' = 1$ at $\overline{d} = \overline{d}_{\max}$. The six resulting $S'(d')$ curves were obviously not identical, but they possessed the same general negatively skewed shape with $S' = 1$ near $d' = 0.55-0.8$ (Figure 6a). This shape shows that an offshore propagating bar increases in amplitude until it has moved through some 55 to 80% of the bar depth zone and that bar decay is, accordingly, confined to a rather narrow (the lower 20 to 45% of the bar depth zone) depth range.

[21] The $S'(d')$ curve averaged over all six sites was approximated reasonably well with a negatively skewed, Gaussian-like function (Figure 6, $r = 0.98$)

$$S' = \exp\left[\frac{-\{(1-d')^a - b\}^2}{c}\right], \qquad (9)$$

in which the values of the parameters a, b, and c, determined with nonlinear least squares fitting by the Gauss-Newton method, are (±95% confidence interval) 0.53 (±0.05), 0.57 (±0.03), and 0.09 (±0.01), respectively. Rewriting (9) into dimensional bar amplitude results in

$$S(\overline{d}) = \delta + (S_{\max} - \delta) \exp\left[\frac{-\left\{\left(1 - \frac{\overline{d} - \overline{d}_{\text{shore}}}{\overline{d}_{\text{sea}} - \overline{d}_{\text{shore}}}\right)^{0.53} - 0.57\right\}^2}{0.09}\right] \qquad (10)$$

Because $S_{\max}$ can be written in terms of $\overline{d}_{\text{sea}}$ (that is, Figure 5) and δ is a constant, $S(\overline{d})$ is determined by $\overline{d}_{\text{shore}}$ and $\overline{d}_{\text{sea}}$ only. In other words, the similarity in the depth dependence of bar amplitude is controlled by two variables, namely the mean depth where the bar zone starts ($\overline{d}_{\text{shore}}$) and where it ends ($\overline{d}_{\text{sea}}$). The dependence of $\overline{d}_{\text{shore}}$ and $\overline{d}_{\text{sea}}$ on various environmental characteristics suggested in section 1 to affect geometric bar parameters is investigated in section 5.

4.1.2. Bar Length

[22] In the cross-shore evolution of bar length at the four Dutch sites, some small intrasite differences were found that were similar to those found for the envelope of bar amplitude. These differences were largely absent in the depth dependence of bar length, indicating that also bar length is a function of mean depth rather than of cross-shore distance. Figure 7 shows the site-averaged L, binned according to $\overline{d} \pm 0.05$ m, together with L at Duck and Hasaki. The symbols from the six sites cannot be discerned well, implying intersite $L(\overline{d})$ differences to be small. Except at Hasaki, L
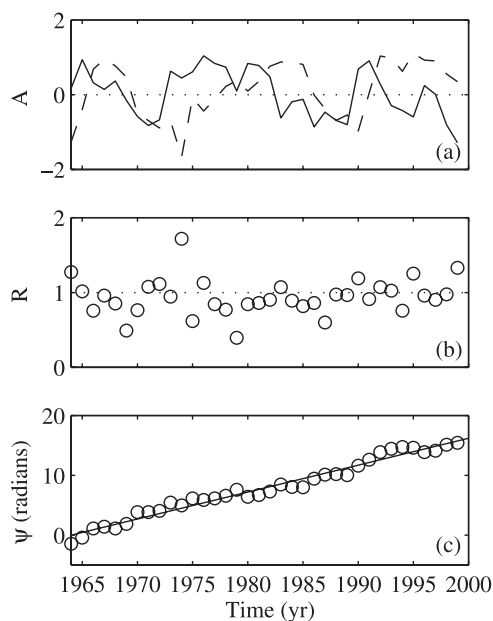
Figure 3. Time series of (a) normalized real (solid) and imaginary (dashed) part of coefficients A, (b) normalized temporal variations R in the bar amplitude, and (c) unwrapped temporal phase ψ of the first CEOF in the example window ($y = 41.50$ km, Noord-Holland). The solid line in Figure 3c is the least squares linear fit.
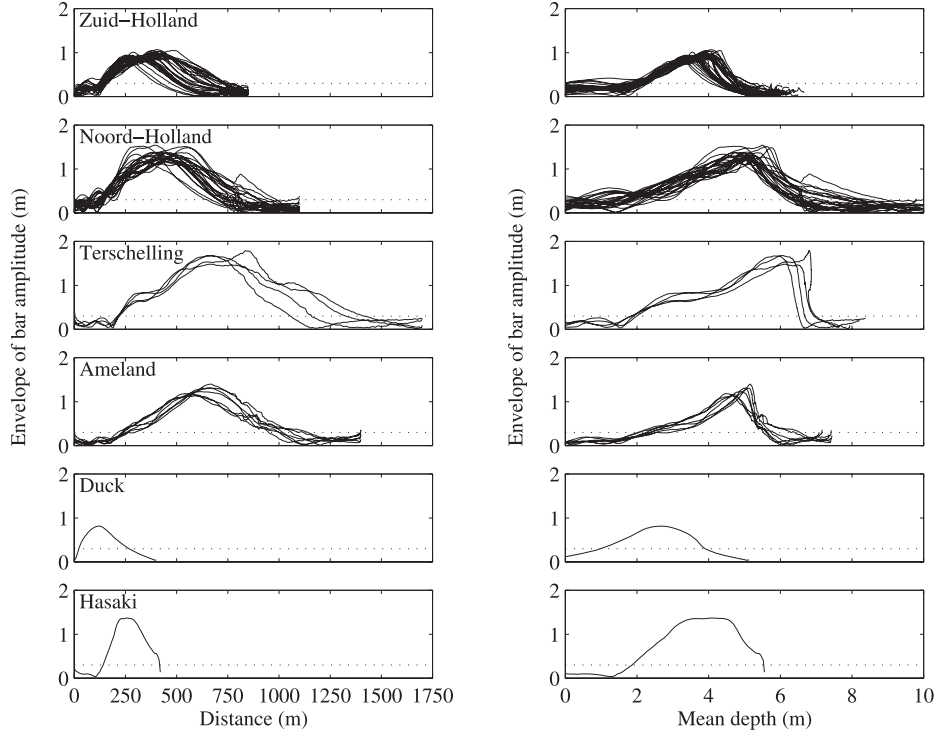
Figure 4. Envelope of bar amplitude S versus (left) cross-shore distance x and (right) mean depth $\overline{d}$. The dotted line in each panel is the threshold $S = 0.3$ m to separate the barred and nonbarred parts of the profile.

increases stronger than linear from ≈ 200 m in $\overline{d} = 2-3$ m to $\approx 500-700$ m in $\overline{d} = 6-7$ m. The scatter in L increases somewhat in the deeper parts of the bar zone. At Hasaki L is about $50-100$ m smaller than at the other sites. The data in Figure 7 can be approximated well ($r = 0.87$) by an exponential curve

$$L(\overline{d}) = a \exp(b\overline{d}), \qquad (11)$$

in which the values of the parameters a and b are 100 (± 8.5) and 0.27 (± 0.02), respectively. The use of an exponential fit is qualitatively consistent with the findings of *Saylor and Hands* [1970] and *Pruszak et al.* [1997], see section 1, although in these papers the dependence was on cross-shore distance rather than on mean depth.

4.1.3. Reconstruction

[23] In the preceding subsections we have derived intersite averaged parameterizations of the bar amplitude S and bar length L. These parameterizations resulted from a number of successive statistical analyses, from CEOF analysis through alongshore and intersite averaging to the Gaussian and exponential fits of equations (10) and (11). It is therefore illustrative to see how well the final parameters are still representative of the original data $\tilde{z}_b(t, x)$. This will be pursued for the same example window as used in section 3.

[24] In this window the cross-shore distribution of S and θ estimated with equations (10) and (11) (using $\overline{d}_{\text{sea}}$, $\overline{d}_{\text{shore}}$, and $\overline{z}_b(x)$) closely resemble S and θ based on CEOF mode 1 (Figures 8a–8b). With these estimated $S(x)$ and $\theta(x)$, and the CEOF mode 1 values of $R(t)$ and $\psi(t)$ (Figure 3), $\tilde{z}_{\text{bar}}(t, x)$ was reconstructed using equation (3). As can be seen by comparing Figure 1c to Figure 1a, the reconstructed perturbations resemble the measured perturbations well; they explain about equal amounts of variance as the perturbations based entirely on CEOF mode 1 (Figure 8c). The use of $R = 1$ in the reconstruction of $\tilde{z}_{\text{bar}}(t, x)$ with equation (3) instead of the time-varying R values of Figure 3b has little effect on the explained variance (Figure 8c). Results similar to Figure 8 were obtained for all windows at all other sites

Table 2. Bar Zone Characteristics

	x_{shore}, m	x_{sea}, m	$\overline{d}_{\text{shore}}$, m	$\overline{d}_{\text{sea}}$, m	x_{bz}, m	$\overline{d}_{\text{bz}}$, m	S_{max}, m	x_{max}, m	$\overline{d}_{\text{max}}$, m	T_r, years
Zuid-Holland[a]	135	603	1.94	4.59	468	2.65	0.93	350	3.71	3.9
Noord-Holland[a]	119	794	1.40	7.02	675	5.62	1.33	444	5.08	15.1
Terschelling[a]	214	1243	1.86	6.79	1029	4.93	1.66	704	6.20	11.4
Ameland[a]	246	1040	2.34	5.89	794	3.55	1.25	619	4.86	6.1
Duck	20	270	0.85	3.92	250	3.07	0.81	120	2.67	113.3 (5.9)[b]
Hasaki	140	415	1.85	5.52	275	3.67	1.37	255	4.07	1.0

[a]Window-averaged values.
[b]South (north) of FRF pier; see text for further explanation.
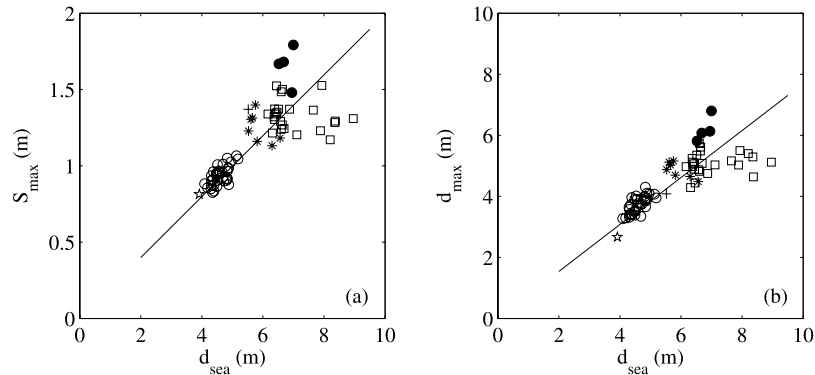
Figure 5. Plots of (a) S_{max} and (b) $\overline{d}_{max}$ versus $\overline{d}_{sea}$ at Zuid-Holland (open circle), Noord-Holland (square), Terschelling (solid dot), Ameland (asterisk), Duck (pentagram), and Hasaki (plus). The solid lines are least squares linear fits given by $S_{max} = 0.20\,\overline{d}_{sea}$ and $\overline{d}_{max} = 0.77\,\overline{d}_{sea}$, respectively. See also Table 3.

except at Hasaki because of the systematic L overestimation when using equation (11) at this site (Figure 7). On the whole these results show that $S(x)$ and $L(x)$ can be predicted accurately (relative to the accuracy of CEOF mode 1) at individual cross-shore transects on the basis of alongshore and intersite averaged parameterizations of $S(d)$ and $L(d)$ given a priori knowledge of $\overline{d}_{sea}$, $\overline{d}_{shore}$, and $\tilde{z}_b(x)$.

4.2. Temporal Characteristics

[25] Return periods T_r of the long-term offshore directed bar cycle ranged from about 1 year at Hasaki to 15 years at Noord-Holland (Table 2). Considerable intrasite variability in T_r was found at Zuid-Holland, Noord-Holland, and Duck. In the two Dutch regions, this variability was related to a long-term three-dimensional type of bar behavior [*Wijnberg and Wolf*, 1994] known as bar switching [*Shand and Bailey*, 1999; *Shand et al.*, 2001]. It involves bars being discontinuous in the alongshore, with a well-developed outer bar on one side of the discontinuity attaching to the inner bar on the other side. On opposite sides of a bar switching area T_r values are about the same and the r^2 of the least squares linear fit between the unwrapped ψ_1 and t exceeds 0.95. Within a switching area bars do not progress systematically in the offshore direction [*Wijnberg and Wolf*, 1994; *Shand et al.*, 2001]. Because T_r quantifies the offshore progression cycle, it is not a meaningful number in a switching area and, accordingly, T_r estimates in switching areas were not used in the computation of the Noord-Holland and Zuid-Holland averaged T_r listed in Table 2.

[26] At Duck T_r amounted to 5.9 years north of the pier, but was only 3.3 years south of the pier (Table 2). In early 1985 and in 1992 the bar system in the south migrated seaward (ψ_1 increased, Figure 9), whereas the bar system to the north did not (ψ_1 remained about constant, Figure 9). As a consequence, the number of interannual bar cycles observed in the north was about half compared to the number in the south.

[27] The only (site-averaged) geometric parameter to show a significant (at the 99% level) linear association with T_r is the bar zone depth range $\overline{d}_{bz}$. Figure 10 shows that T_r increases with $\overline{d}_{bz}$ by ~ 4 year/m ($r = 0.89$). The largest outlier is Hasaki, where measured (Table 2) and predicted (Figure 10) T_r differ by about 5 years. Without the Hasaki data point the slope of the least squares linear fit remains unaltered but r improves to 0.98.

5. Environmental Characteristics

[28] In the preceding section we have shown that considerable intersite differences exist in $S(\overline{d})$ and T_r. The similarity in $S(\overline{d})$ can be described largely in terms of $\overline{d}_{shore}$ and $\overline{d}_{sea}$ (equation (10)), and T_r is positively associated with the difference between these two depths, $\overline{d}_{bz}$ (Figure 10). In this section we investigate whether simple bulk statistics of various environmental characteristics that have been suggested in the literature to affect bar dynamics, or morpho-

Table 3. Correlation Coefficients of Least Squares Linear Fits[a]

	x_{shore}	x_{sea}	$\overline{d}_{shore}$	$\overline{d}_{sea}$	x_{bz}	$\overline{d}_{bz}$	S_{max}	x_{max}	$\overline{d}_{max}$
x_{shore}	1	0.55	0.74	(−0.02)	0.37	(−0.29)	(0.29)	0.66	0.33
x_{sea}		1	(−0.04)	0.68	0.98	0.55	0.71	0.89	0.83
$\overline{d}_{shore}$			1	−0.44	(−0.23)	−0.71	(−0.16)	(0.10)	(−0.17)
$\overline{d}_{sea}$				1	0.76	0.95	0.78	0.50	0.82
x_{bz}					1	0.68	0.71	0.83	0.84
$\overline{d}_{bz}$						1	0.67	0.36	0.71
S_{max}							1	0.68	0.92
x_{max}								1	0.84
$\overline{d}_{max}$									1

[a]Values not significant at the 99% confidence level are shown in parentheses.
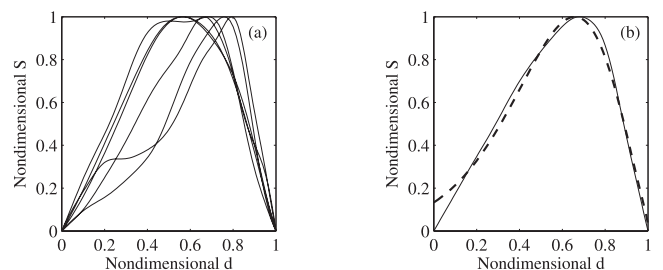
Figure 6. (a) Site-averaged normalized bar amplitude S' versus normalized mean depth d' and (b) average of the six S' curves shown in Figure 6a (solid line) and exponential fit given by equation (9) (dashed line).
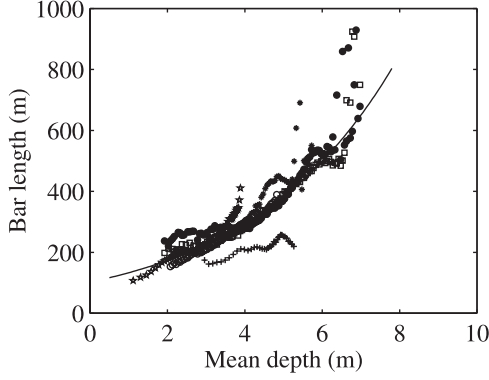
Figure 7. Bar length L versus mean depth $\overline{d}$ at all six sites. Same symbol use as in Figure 5.

dynamic variability in general, are associated with the intersite differences in $\overline{d}_{shore}$, $\overline{d}_{sea}$, and $\overline{d}_{bz}$.

[29] Environmental characteristics at the various sites are listed in Table 4 and include the mean slope $\beta = \overline{d}_{bz}/x_{bz}$ of the barred part of the profile, the median grain size D_{50}, the 'storm' breaker height H_b and peak period T_p, the low-tide level η_{LT} with respect to mean sea level, the tide range $\Delta\eta = \eta_{HT} - \eta_{LT}$, where η_{HT} is the high-tide level, the nondimensional fall velocity $\Omega = H_b/(w_s T_p)$, where w_s is the median fall velocity, and the relative tide range $RTR = \Delta\eta/H_b$ [*Masselink and Short*, 1993]. The D_{50} is often not constant in the cross shore [e.g., *Gallagher et al.*, 1998; *Guillén and Hoekstra*, 1997; *Katoh and Yanagishima*, 1995] and the values in Table 4 represent midnearshore values. The storm H_b and T_p were quantified as the 0.99 quantile of time series of H_b and T_p, where the H_b time series were computed from long-term, hourly to two-hourly sampled offshore wave records collected at each site (see Table 4) using linear wave theory

$$H_b = \left(\frac{\gamma}{g}\right)^{1/5} \left[H_0^2 c_{g0} \cos\theta_0\right]^{2/5}, \qquad (12)$$

where H_0, c_{g0}, and θ_0 are the offshore root mean square wave height, group velocity and angle of incidence, respectively. The breaker parameter γ was set to 0.4 [*Thornton and Guza*, 1982]. At Zuid-Holland and Hasaki $\theta_0 = 0$ was assumed because wave direction estimates were not available. Values of η_{LT} and η_{HT} were computed as the 0.05 and 0.95 quantile of long-term water level records obtained at each site (see Table 4), respectively. As can be deduced from Table 4, intersite differences exist for all environmental characteristics except D_{50}.

[30] Linear regression results (Table 5)] were found to be inconclusive because the magnitude of r was often influenced strongly by the data from an individual site. In several cases r was not statistically significant at the 95% using data from all six sites, but removal of one of the sites resulted in the appearance of a significant dependence among the remaining sites. An example hereof is the improvement of r from -0.62 to -0.83 for η_{LT} and $\overline{d}_{shore}$ without the Hasaki data. Even more marked is the improvement of $r = 0.57$ to $r = 0.97$ for $\overline{d}_{sea}$ and the storm H_b, and from $r = 0.33$ to $r = 0.89$ for $\overline{d}_{bz}$ and the storm H_b after removal of the Noord-

Holland data. Thus, among a subset of the data there is the tendency of the bar zone to begin in deeper water with lower low-tide levels, of the bar zone to end in deeper water (and thus of the bars to reach a larger maximum amplitude) with an increase in the storm H_b, and of the bar zone range (and thus T_r; Figure 10) to increase with an increase in storm H_b as well. The negative association between $\overline{d}_{shore}$ and η_{LT} may essentially reflect the subtidal nature of the studied bar systems, and the positive association between $\overline{d}_{sea}$ and H_b is qualitatively consistent with results from laboratory experiments [*King*, 1959; *Larson and Kraus*, 1989] and previous field observations [*Davidson-Arnott*, 1988]. We do not find the often suggested relationship that bars become less accentuated with an increase in tide range [*Wright et al.*, 1987; *Masselink and Short*, 1993]; it is, however, possible that this trend manifests itself at (relative) tide ranges larger than included in the present data. Also, β, T_p, Ω, and RTR do not appear to control geometric and temporal bar parameters.

[31] The positive dependence of $\overline{d}_{bz}$ on storm H_b is qualitatively consistent with results of the comparative study by *Shand et al.* [1999]. We do note, however, that our return period T_r is not identical to their bar period, defined as the time period between the onset of offshore migration and final bar decay, albeit that both periods are strongly related [*Shand et al.*, 1999, Figure 9]. Interestingly, *Shand et al.* [1999] also had to remove data from Noord-Holland to find the positive association between their period and H_b. We cannot confirm their suggestion of a relation-
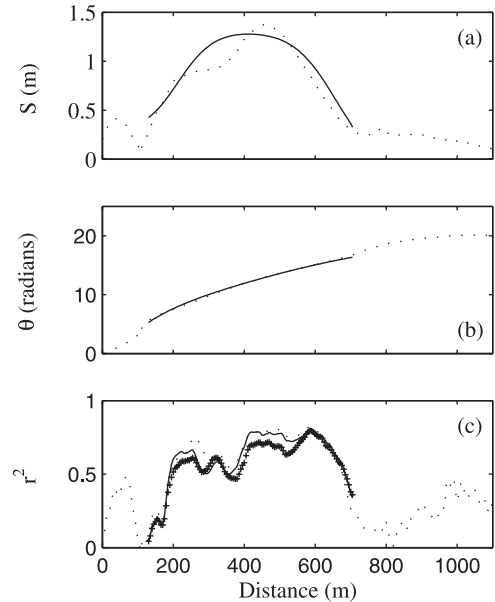
Figure 8. The solid lines represent (a) the envelope of the bar amplitude S based on equation (10), (b) the unwrapped spatial phase θ based on equation (11), and (c) the variance r^2 explained by $\tilde{z}_{bar}(t, x)$ reconstructed (equation (3)) with the estimated $S(x)$ and $\theta(x)$ and the CEOF mode 1 values of $R(t)$ and $\psi(t)$ versus cross-shore distance in the example data set at $y = 41.50$ km in Noord-Holland, Netherlands. The dotted line in each plot shows the results of CEOF mode 1 (see Figure 2). The symbols in Figure 8c are the variance explained by $\tilde{z}_{bar}(t, x)$ using $R = 1$ in equation (3).
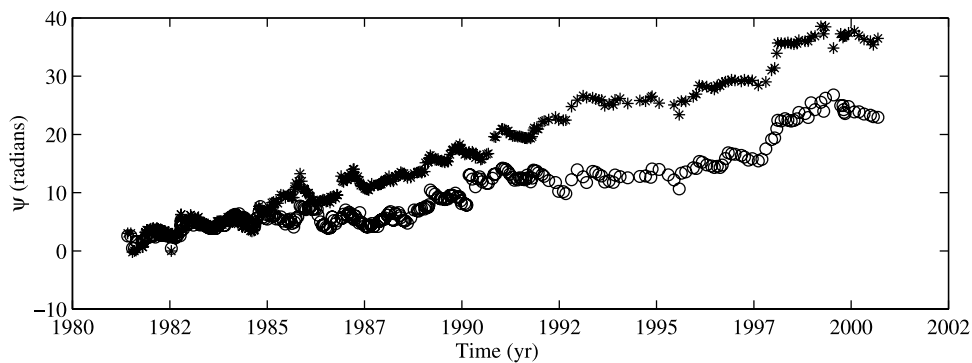
Figure 9. Time series of temporal phase ψ at Duck in $y = -92$ m (asterisks) and $y = 1096$ m (circles).

ship between β and T_r, either with or without the Noord-Holland data ($r = -0.17$ and -0.26, respectively).

6. Discussion

[32] In this paper we have shown through an analysis of six long-term bathymetric data sets that sandbars share common nondimensional amplitude characteristics, but considerable intersite variation in absolute dimensions and return intervals. The key geometric parameters that steer this intersite variation are the time-averaged mean depths at the shoreward and seaward side of the bar zone, as well as their difference. Although our results confirm the many literature suggestions on the similarity in geometric bar parameters (see section 1), we are unaware of existing theories that could have a priori predicted the dependence of bar amplitude and length on mean depth as found here. Hopefully, our empirical results will stimulate new model conceptualization and can be used for future model fitting and validation.

[33] The intersite variability in geometric and temporal bar parameters do not mirror intersite differences in external forcing conditions conclusively. Among a subset of the sites $\overline{d}_{shore}$ tends to increase with lower low-tide levels, and $\overline{d}_{sea}$ and $\overline{d}_{bz}$ tend to increase with the 99% quantile of the root

mean square breaker height. These relationships should, however, be considered with care. Not only is our data set limited in size, the intersite variability in low-tide levels and breaker height is also small compared to the wide range of geometric and temporal bar parameters. It is difficult to envisage why, for instance, the only 40-cm difference in the breaker height between Duck and Terschelling should lead to an approximate 300-cm change in the depth at the seaward end of the bar zone. If we assume that the depth at breaking is given by H_b/γ, then with $\gamma = 0.4$ (section 5) a 100-cm change is expected only.

[34] The attempt to couple intersite variability in bed profile characteristics to environmental parameters essentially tested whether interannual sandbar behavior is a forced (that is, because of external forcing factors) type of behavior. The inconclusive nature of the regression results could mean that the link with the forcing is more complex than the linear relationships investigated here, that other aspects of the forcing not accounted for here are responsible, or that interannual bar behavior is the manifestation of the free (that is, nonforced) behavior of a nonlinear random dissipative system. In fact, recent studies [e.g., *De Vriend*, 1998; *Southgate and Möller*, 2000; *Werner*, 1999] have pointed out that the nearshore system has the key characteristics to exhibit free behavior: the nearshore system is highly dimensional and strongly nonlinear, it receives a continuous, stochastically forced input of energy which is dissipated within the system, and it contains morphologic
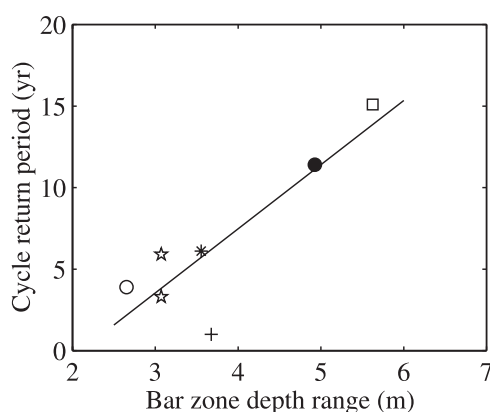
Figure 10. Site-averaged cycle return period T_r versus site-averaged bar zone depth range $\overline{d}_{bz}$ (same symbol usage as in Figure 5). Estimates of T_r south and north of the FRF pier at Duck are both shown and were also both included in the linear regression analysis. The solid line is least squares linear fit ($r = 0.89$, slope = 4 yr/m).

Table 4. Environmental Characteristic

Region	D_{50}[a], μm	β	H_b,[b] m	T_p,[b] s	η_{LT},[c] m	$\Delta\eta$,[c] m	Ω	RTR
Zuid-Holland	170	1:170	2.58	9.0	−0.85	1.9	14.3	0.72
Noord-Holland	210	1:120	2.55	9.3	−0.96	1.9	9.9	0.74
Terschelling	180	1:205	2.87	11.4	−1.27	2.3	11.5	0.79
Ameland	180	1:225	2.67	10.0	−1.28	2.4	12.2	0.89
Duck	180	1:80	2.47	15.4	−0.54	1.4	7.3	0.55
Hasaki	175	1:75	2.72	13.4	−0.54	1.1	9.7	0.42

[a]Zuid-Holland, *Terwindt* [1962]; Noord-Holland and Ameland, *Stolk* [1989]; Terschelling, *Guillén and Hoekstra* [1997]; Duck, *Gallagher et al.* [1998]; and Hasaki, *Katoh and Yanagishima* [1995].

[b]Zuid-Holland, measurement platform Noordwijk; Noord-Holland, buoy IJmuiden Munitiestortplaats; Terschelling, buoy Terschelling; Ameland, buoy Schiermonnikoog; Duck, buoy 630; Hasaki, ultrasonic sensor Kashima Port [*Nagai et al.*, 1994].

[c]Zuid-Holland, measurement platform Noordwijk; Noord-Holland, tide station Petten Zuid; Terschelling, tide station Terschelling Noordzee; Ameland, tide station Wierumergronden; Duck, tide station 111; Hasaki, tide station at tip of HORS pier.

Table 5. Correlation Coefficients of Least Squares Linear Fits[a]

	β	H_b	T_p	η_{LT}	$\Delta\eta$	Ω	RTR
$\overline{d}_{shore}$	−0.64	0.62	−0.60	−0.62	0.56	0.79	0.49
$\overline{d}_{sea}$	−0.43	0.57	−0.51	−0.66	0.53	0.16	0.46
$\overline{d}_{bz}$	−0.17	0.33	−0.27	−0.42	0.32	−0.19	0.27

[a]None of the correlation coefficients are significant at the 95% confidence level.

feedback, as changes in depth give rise to changes in waves and currents. Furthermore, *De Vriend* [1998] speculated that the occasionally different behavior at either side of the FRF pier could be considered as the jumping of the system between different states and *Southgate and Möller* [2000] suggested profile evolution at Duck within a 15–40-month time window to have fractal properties, characteristics of behavior exhibited by nonlinear random dissipative systems. However, our negative result in the link with forcing and the existing literature suggestions [*De Vriend*, 1998; *Southgate and Möller*, 2000] can only be considered as circumstantial evidence that interannual bar behavior is the free behavior of a stochastically forced, nonlinear random system.

7. Conclusions

[35] We have quantified geometric and long-term temporal characteristics of six natural bar systems (Zuid-Holland, Noord-Holland, Terschelling, Ameland, Duck, and Hasaki) that exhibit long-term offshore directed migration. The first mode of a complex empirical orthogonal function analysis of the demeaned bathymetric data typically accounted for 60–75% of the depth variance and resulted in objective descriptions of bar amplitude, bar length, and cycle return period. On the basis of a bar amplitude threshold of 0.3 m, the barred part of the profile was separated from the shoreward and seaward nonbarred parts. Considerable intersite differences exist in the mean depths at the shoreward and seaward side of the bar zone ($\overline{d}_{shore}$ and $\overline{d}_{sea}$), as well as in the maximum bar amplitude and in the mean depth where the bar amplitude is maximum. The evolution of bar amplitude with mean depth is similar for all sites and can be described empirically ($r = 0.98$) by a negatively skewed Gaussian function. Bar lengths increase exponentially with depth ($r = 0.87$) and, for a given depth, are identical at all sites except at Hasaki where bar lengths tend to be 50–100 m shorter. Cycle return periods, ranging from 1 year at Hasaki to 15 year at Noord-Holland, increase linearly ($r = 0.89$) with the difference $\overline{d}_{shore} - \overline{d}_{sea}$.

[36] Results of a linear regression analysis between geometric bar parameters and bulk statistics of wave, tide, sediment, and bed profile characteristics are inconclusive, because the magnitude of r often depended strongly on the data from an individual site. Among a subset of the data there is the tendency of $\overline{d}_{shore}$ to increase with lower low-tide levels ($r = -0.83$), reflecting the subtidal nature of the studied bar systems, and of $\overline{d}_{sea}$ and $\overline{d}_{bz}$ to increase with the 99% quantile of the root mean square breaker height ($r = 0.97$ an 0.89, respectively), qualitatively consistent with earlier laboratory experiments and field observations. Other environmental characteristics, like the profile slope, the nondimensional fall velocity, and the relative tide range,

do not appear to control intersite differences in geometric and long-term temporal bar variability.

References

Barnett, T. P., Interaction of the monsoon and Pacific trade wind system at interannual time scales. part I: The equatorial zone, *Mon. Weather Rev.*, *111*, 756–773, 1983.

Davidson-Arnott, R. G. D., Controls on formation and form of barred nearshore profiles, *Geogr. Rev.*, *78*, 185–193, 1988.

De Vriend, H. J., On the predictability of coastal morphology, paper presented at 3rd European Marine Science and Technology Conference, Eur. Comm., Lisbon, Portugal, 1998.

Evans, O. F., The low and ball of the eastern shore of Lake Michigan, *J. Geol.*, *48*, 476–511, 1940.

Gallagher, E. L., S. Elgar, and R. T. Guza, Observations of sand bar evolution on a natural beach, *J. Geophys. Res.*, *103*, 3203–3215, 1998.

Greenwood, B., and R. G. D. Davidson-Arnott, Marine bars and nearshore sedimentary processes, Kouchibouguac Bay, New Brunswick, Canada, in *Nearshore Sediment Dynamics and Sedimentation*, vol. 16, edited by J. Hails and A. Carr, pp. 123–150, John Wiley, Hoboken, N.J., 1975.

Guillén, J., and P. Hoekstra, Sediment distribution in the nearshore zone: Grain size evolution in response to shoreface nourishment (Island of Terschelling, the Netherlands), *Estuarine Coastal Shelf Sci.*, *45*, 639–652, 1997.

Horel, J. D., Complex principal component analysis: Theory and examples, *J. Clim. Appl. Meteorol.*, *23*, 1660–1673, 1984.

Katoh, K., Hazaki Oceanographical Research Station (HORS), *Mar. Technol. Soc. J.*, *31*, 49–56, 1998.

Katoh, K., and S. Yanagishima, Changes of sand grain distribution in the surf zone, in *Coastal Dynamics '95: Proceedings of the International Conference on Coastal Research in Terms of Large Scale Experiments: Gdansk, Poland September 4–8, 1995*, edited by R. B. Zeidler and W. R. Dally, pp. 639–650, Am. Soc. of Civ. Eng., Reston, Va., 1995.

Keulegan, G. H., An experimental study of submarine sand bars, *Tech. Rep. 3*, Beach Erosion Board, Off. of the Chief of Eng., U.S. Army Eng. Waterw. Export Stn., Vicksburg, Miss., 1948.

King, C. A. M., *Beaches and Coasts*, Edward Arnold, London, 1959.

King, C. A. M., and W. W. Williams, The formation and movement of sand bars by wave action, *Geogr. J.*, *113*, 69–85, 1949.

Kuriyama, Y., Medium-term bar movement and sediment transport at HORS, *Tech. Rep. 39, 4*, Port and Harbour Res. Inst., Yokosuka, Japan, 2000.

Kuriyama, Y., Medium-term bar behavior and associated sediment transport at Hasaki, Japan, *J. Geophys. Res.*, *107*(C9), 3132, doi:10.1029/2001JC000899, 2002.

Kuriyama, Y., and J. H. Lee, Medium-term beach profile change on a bar-trough region at Hasaki, Japan, investigated with complex principal component analysis, in *Coastal Dynamics '01: Proceedings of the Fourth Conference on Coastal Dynamics, June 11–15, 2001, Lund Sweden*, edited by H. Hanson and M. Larson, pp. 959–968, Am. Soc. of Civ. Eng., Reston, Va., 2001.

Larson, M., and N. C. Kraus, SBEACH: Numerical model for simulating storm-induced beach change, report 1. Empirical foundation and model development, *Tech. Rep. CERC-89-9*, Dep. of the Army, U.S. Army Corps of Eng., Vicksburg, Miss., 1989.

Larson, M., and N. C. Kraus, Temporal and spatial scales of beach profile change, Duck, North Carolina, *Mar. Geol.*, *117*, 75–94, 1994.

Lippmann, T. C., R. A. Holman, and K. K. Hathaway, Episodic, nonstationary behavior of a two sand bar system at Duck, NC, USA, *J. Coastal Res.*, *SI*(15), 49–75, 1993.

Masselink, G., and A. D. Short, The effect of tide range on beach morphodynamics and morphology: A conceptual beach model, *J. Coastal Res.*, *9*, 785–800, 1993.

Nagai, T., K. Sugahara, N. Hashimoto, T. Asai, S. Higashiyama, and K. Toda, Introduction of Japanese NOWPHAS system and its recent topics, paper presented International Conference on Hydro-Technical Engineering for Port and Harbor Construction, Port and Harbour Res. Inst., Kobe, Japan, 1994.

North, G. R., T. L. Bell, R. F. Cahalan, and F. J. Moeng, Sampling errors in the estimation of empirical orthogonal functions, *Mon. Weather Rev.*, *110*, 699–706, 1982.

Plant, N. G., R. A. Holman, M. H. Freilich, and W. A. Birkemeier, A simple model for interannual sandbar behavior, *J. Geophys. Res.*, *104*, 15,755–15,776, 1999.

Plant, N. G., M. H. Freilich, and R. A. Holman, Role of morphologic feedback in surf zone sandbar response, *J. Geophys. Res.*, *106*, 973–989, 2001.

Pruszak, Z., and G. Różyński, Variability of multiple profiles in terms of random sine functions, *J. Waterw. Port Coastal Ocean Eng.*, *124*, 48–56, 1998.

Pruszak, Z., G. Różyński, and R. B. Zeidler, Statistical properties of multiple bars, *Coastal Eng.*, *31*, 263–280, 1997.

Ruessink, B. G., and A. Kroon, The behaviour of a multiple bar system in the nearshore zone of Terschelling: 1965–1993, *Mar. Geol.*, *121*, 187–197, 1994.

Ruessink, B. G., R. A. Holman, and K. M. Wijnberg, Interannual nearshore bar behaviour: An intersite comparison, in *Coastal Dynamics '01: Proceedings of the Fourth Conference on Coastal Dynamics, June 11–15, 2001, Lund Sweden*, edited by H. Hanson and M. Larson, pp. 646–655, Am. Soc. of Civ. Eng., Reston, Va., 2001.

Saylor, J. H., and E. B. Hands, Properties of longshore bars in the Great Lakes, paper presented at 12th International Conference on Coastal Engineering, Am. Soc. of Civ. Eng., Washington, D.C., 1970.

Shand, R. D., and D. G. Bailey, A review of net offshore bar migration with photographic illustrations from Wanganui, New Zealand, *J. Coastal Res.*, *15*, 365–378, 1999.

Shand, R. D., D. G. Bailey, and M. J. Shephard, An inter-site comparison of net offshore bar migration characteristics and environmental conditions, *J. Coastal Res.*, *15*, 750–765, 1999.

Shand, R. D., D. G. Bailey, and M. J. Shephard, Longshore realignment of shore-parallel sand-bars at Wanganui, New Zealand, *Mar. Geol.*, *179*, 147–161, 2001.

Shepard, F. P., Longshore-bars and longshore-troughs, *Tech. Rep. 15*, Beach Erosion Board, Off. of the Chief of Eng., U.S. Army Eng. Waterw. Export Stn., Vicksburg, Miss., 1950.

Southgate, H. N., and I. Möller, Fractal properties of coastal profile evolution at Duck, North Carolina, *J. Geophys. Res.*, *105*, 11,489–11,507, 2000.

Stolk, A., Zandsysteem kust, een morfologische karakterisering (in Dutch), *Geopro Rep. 1989.02*, 97 pp., Vakgroep Fysische Geogr., Rijksuniv., Utrecht, Netherlands, 1989.

Terwindt, J. H. J., Study of grain size variations at the coast of Katwijk (in Dutch), *Tech. Rep. K-324*, Rijkswaterstaat, The Hague, 1962.

Thornton, E. B., and R. T. Guza, Energy saturation and phase speeds measured on a natural beach, *J. Geophys. Res.*, *87*, 9499–9508, 1982.

Von Storch, H., and F. W. Zwiers, *Statistical Analysis in Climate Research*, Cambridge Univ. Press, New York, 1999.

Werner, B. T., Complexity in natural landform patterns, *Nature*, *284*, 102–104, 1999.

Wijnberg, K. M., Large scale, decadal behaviour of nearshore morphology: Three case studies of multiple barred coasts, in *Geographical Developments in Coastal Morphodynamics: A Tribute to Joost Terwindt*, edited by A. Kroon and B. G. Ruessink, pp. 185–203, Elinkwijk, Utrecht, Netherlands, 1998.

Wijnberg, K. M., and J. H. J. Terwindt, Extracting decadal morphological behaviour from high-resolution, long-term bathymetric surveys along the Holland coast using eigenfunction analysis, *Mar. Geol.*, *126*, 301–330, 1995.

Wijnberg, K. M., and F. C. J. Wolf, Three-dimensional behaviour of a multiple bar system, in *Coastal Dynamics '94: Proceedings of an International Conference on the Role of the Large Scale Experiments in Coastal Research: Universitat Polite*, edited by A. S. Arcilla, N. C. Kraus, and M. J. F. Stive, pp. 59–73, Am. Soc. of Civ. Eng., 1994.

Wright, L. D., A. D. Short, J. D. Boon, S. Kimball, and J. H. List, The morphodynamic effect of incident wave groupiness and tide range on an energetic beach, *Mar. Geol.*, *74*, 1–20, 1987.

Zenkovich, V. P., *Processes of Coastal Development*, Oliver and Boyd, White Plains, N.Y., 1967.

————————————

R. A. Holman, Coastal Imaging Laboratory, College of Oceanic and Atmospheric Sciences, Oregon State University, Corvallis, OR 97331-5503, USA. (holman@coas.oregonstate.edu)

Y. Kuriyama, Littoral Drift Division, Marine Environment and Engineering Department, Port and Airport Research Institute, Nagase 3-1-1, Yokosuka, Kanagawa 239-0826, Japan. (kuriyama@pari.go.jp)

B. G. Ruessink and I. M. J. van Enckevort, Institute for Marine and Atmospheric Research, Department of Physical Geography, Utrecht University, P. O. Box 80.115, 3508 TC Utrecht, Netherlands. (g.ruessink@geog.uu.nl; i.vanenckevort@geog.uu.nl)

K. M. Wijnberg, WL|Delft Hydraulics, Marine and Coastal Management, P. O. Box 177, 2600 MH Delft, Netherlands. (kathelijne.wijnberg@wldelft.nl)